Weak electronic correlations and absence of heavy-fermion state in KNi_2Se_2

Q. Fan,[1,2,*] X. P. Shen,[1,2,*] M. Y. Li,[3] D. W. Shen,[3,†] W. Li,[3] X. M. Xie,[3] Q. Q. Ge,[1,2] Z. R. Ye,[1,2] S. Y. Tan,[1,2] X. H. Niu,[1,2] B. P. Xie,[1,2] and D. L. Feng[1,2,‡]

[1]*State Key Laboratory of Surface Physics, Department of Physics, and Advanced Materials Laboratory, Fudan University, Shanghai 200433, People's Republic of China*

[2]*Collaborative Innovation Center of Advanced Microstructures, Fudan University, Shanghai 200433, China*

[3]*State Key Laboratory of Functional Materials for Informatics, Shanghai Institute of Microsystem and Information Technology (SIMIT), Chinese Academy of Sciences, Shanghai 200050, People's Republic of China*

(Received 4 December 2014; revised manuscript received 14 February 2015; published 9 March 2015)

We have studied the low-lying electronic structure of a new $ThCr_2Si_2$-type superconductor KNi_2Se_2 with angle-resolved photoemission spectroscopy. Three bands intersect the Fermi level, forming complicated Fermi surface topology, which is sharply different from its isostructural superconductor $K_xFe_{2-y}Se_2$. The Fermi surface shows weak variation along the k_z direction, indicating its quasi-two-dimensional nature. Further comparison with the density functional theory calculations demonstrates that there exist relatively weak correlations and substantial hybridization in the low-lying electronic structure. Our results indicate that the large density of states at the Fermi energy leads to the reported mass enhancement based on the specific heat measurements. Moreover, no anomaly is observed in the spectra when entering the fluctuating charge density wave state reported earlier.

DOI: 10.1103/PhysRevB.91.125113 PACS number(s): 74.25.Jb, 74.70.−b, 79.60.−i, 71.20.−b

I. INTRODUCTION

The iron-chalcogenide superconductors $A_xFe_{2-y}Se_2$ (A = K, Rb, etc.) with superconducting transition temperature (T_c) up to 33 K have aroused a great deal of research interest [1–7]. Compared with the iron-pnictide superconductors, $A_xFe_{2-y}Se_2$ exhibits some unique properties, such as the antiferromagnetically ordered insulator parent compound with Fe vacancy order [3–6]. Particularly, angle-resolved photoemission spectroscopy (ARPES) revealed that the Fermi surface of the superconducting phase consists of electron pockets only, raising a serious challenge to the prevalent Fermi surface nesting mechanism for the superconductivity in iron-based superconductors [8,9].

Recently, another chalcogenide superconductor KNi_2Se_2 was reported [10], which shares the same crystal structure and almost the same lattice constants with $K_xFe_{2-y}Se_2$, except that there are no vacancies in KNi_2Se_2 [11]. However, previous experiments indicated that KNi_2Se_2 displays a rich but sharply different phase diagram from that of $K_xFe_{2-y}Se_2$ [10]. Based on the specific heat measurements and neutron pair-distribution-function analysis, KNi_2Se_2 was suggested to show a local charge density wave (CDW) fluctuating state above 20 K, which then enters a coherent heavy-fermion state at lower temperatures. Eventually, it becomes superconducting below ∼0.8 K [10]. The large linear specific heat coefficient (or Sommerfeld coefficient, γ) was proposed to be due to the strong electron correlations and heavy-fermion behavior in KNi_2Se_2. More specifically, mixed valency of the Ni atoms was proposed to induce the heavy effective band mass m^*. On the other hand, we note that the band renormalization factor of $BaNi_2As_2$ (a Ni-based superconductor with $T_c \sim 0.7$ K) is merely ∼1.66, in the weak-interaction regime, and thus the conventional electron-phonon interaction mechanism was suggested to be the cause of the superconductivity therein [12]. In an ionic picture, the Ni orbital configuration is $3d^8$ for $BaNi_2As_2$, and $3d^{8.5}$ for KNi_2Se_2. Consequently, the Hund's rule coupling and electron correlations should be weakened with the increasing number of $3d$ electrons in the latter compound [13], which is inconsistent with the proposed heavy-fermion scenario in KNi_2Se_2. To resolve this controversy and understand the unique properties of KNi_2Se_2, it is critical to study its electronic structure.

In this paper, we have systematically studied the electronic structure of the single-crystalline KNi_2Se_2 with ARPES. There are two electron pockets around the M point: a holelike square pocket surrounding the Γ point, and a holelike narrow racetrack pocket surrounding the X point, respectively. The electronic structure of KNi_2Se_2 shows relatively weak k_z dependence, indicative of its two-dimensional (2D) character. Further comparison between the density functional theory (DFT) band calculations and ARPES data gives a renormalization factor of about 1.54, which indicates that the electron correlations are weak. Furthermore, we find that the Fermi velocities of several bands are relatively small and thus enhance the density of states (DOS) at the Fermi energy (E_F). Our quantitative analysis shows that the large γ of KNi_2Se_2 together with those of $BaNi_2As_2$ and KFe_2As_2 (which has even larger γ), can be well accounted by the multiple large Fermi surfaces and relatively small Fermi velocities in these systems.

II. EXPERIMENT

High-quality single crystals of KNi_2Se_2 were grown by self-flux method with nominal composition K:Ni:Se = 1:2:2. The mixture was loaded into the alumina crucible and then sealed in an argon-filled iron crucible. The entire assembly was kept at 1273 K for three hours, and then cooled down to 873 K slowly at a rate of ∼4 K/h before shutting off the power. The samples are crystallized in the tetragonal $ThCr_2Si_2$-type structure with the space group $I4/mmm$,

*These authors contributed equally to this work.
†dwshen@mail.sim.ac.cn
‡dlfeng@fudan.edu.cn

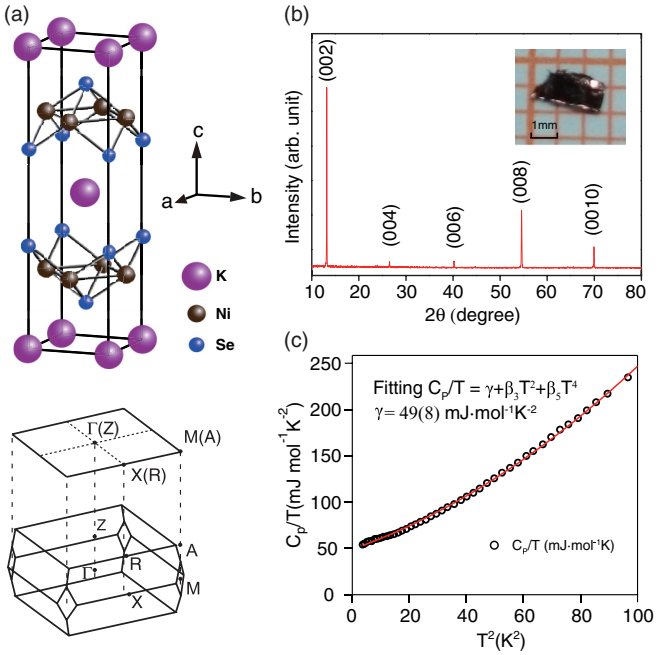

FIG. 1. (Color online) (a) Representative unit cell of KNi_2Se_2 (upper panel) and its Brillouin zone (lower panel). Note one tetragonal unit cell of KNi_2Se_2 contains two chemical formula units. For the convenience, the 2D Brillouin zone is referred hereafter, which is the projection of the three-dimensional Brillouin zone. (b) X-ray diffraction patterns of KNi_2Se_2 single crystal after cleavage. The inset shows the photo of a typical single crystal. (c) The low-temperature specific heat data of KNi_2Se_2 divided by temperature versus temperature squared, revealing a large linear electronic contribution to the low-temperature specific heat.

as shown in Fig. 1(a) [14]. The as-grown single crystals with a typical dimension of $2.5 \times 1.0 \times 0.1$ mm^3 show a flat shiny surface of pink color after cleavage [the inset of Fig. 1(b)]. The electron probe microanalysis measurements across samples with more than ten points indicate that the composition is quite homogeneous, and the averaged stoichiometric ratio is determined to be $KNi_{2.06}Se_{2.01}$. Since this determined composition is close to the stoichiometry, we will still designate the samples as KNi_2Se_2 for convenience hereafter. In Fig. 1(b), x-ray diffraction measurements show that only the series of $(00l)$ narrow reflection peaks appear, suggestive of the good crystalline quality. The low-temperature specific heat [Fig. 1(c)] can be well fitted by the formula $C_p/T = \gamma + \beta_3 T^2 + \beta_5 T^4$ in the temperature range from 1.8 to 10 K, and the resulting large Sommerfield coefficient ($\gamma = 49.8$ mJ mol^{-1} K^{-2}) is in good agreement with previous reports [10,11]. For comparison, we note that the corresponding γ is about 13.2 mJ mol^{-1} K^{-2} for $BaNi_2As_2$ [15], and about 94.3 mJ mol^{-1} K^{-2} for KFe_2As_2 [16].

ARPES measurements were performed at (1) Beamline 7U of the UVSOR synchrotron facility with a MBS A-1 electron analyzer, (2) Beamline 28A of Photon Factory, KEK, Tsukuba, with a Scienta SES-2002 analyzer, and (3) the in-house system equipped with a SPECS UVLS helium discharging lamp and VG Scienta R4000 electron analyzer. The overall energy resolution was set to 15–30 meV depending on the photon energy, and the typical angular resolution was 0.3°. Samples were cleaved *in situ* and then measured under ultrahigh vacuum better than 6×10^{-11} mbar. The sample surfaces were stable and did not show any sign of degradation during the measurements.

The first-principles calculations were implemented in the VASP code [17]. The plane wave basis method and the Perdew-Burke-Ernzerhof [18] exchange correlation potential have been used. Throughout the calculations, a 500 eV cutoff in the plane wave expansion and a $12 \times 12 \times 12$ Monkhorst-Pack $\vec{k}$ grid were chosen to ensure the calculation with an accuracy of 10^{-5} eV. In our calculations, the crystal structure and lattice constants were taken from the experimental values [10,14].

III. EXPERIMENTAL RESULTS

The photoemission intensity map of KNi_2Se_2 at 15 K is shown in Fig. 2(a), which is overlaid on the projected 2D Brillouin zone. The resulting Fermi surface (FS) consists of one squarelike Fermi pocket around the zone center, two Fermi pockets around zone corner, and one narrow racetrack pocket extending to the middle of the zone boundaries, as highlighted by the colored dashed lines. This complicated FS is direct evidence of the multiband behavior in this compound, consistent with previous Hall effect measurement [11] and theoretical calculations [19,20]. Although this multiband character is similar to iron-based superconductors, the detailed FS topology of KNi_2Se_2 is distinct from that of $K_xFe_{2-y}Se_2$, which only exhibits circular electronlike pockets around the zone corner [8,9].

Now we examine the band dispersions of KNi_2Se_2 along several high-symmetry directions as indicated in the lower panel of Fig. 2(a). We chose 75 eV photons to probe the band structure near the ΓXM plane of KNi_2Se_2 considering an inner potential of 15 eV as discussed below. Along Γ-M [cut #1 in Fig. 2(b)], three Fermi crossings can be identified by fitting the corresponding momentum distribution curve (MDC) at E_F. Moreover, the corresponding band dispersions can be tracked with the peaks in the energy distribution curves (EDCs) [Fig. 2(c)], and they are assigned as β, δ_1, and δ_2, respectively. Among them, the holelike β band encloses the Γ point, forming the square-shaped Fermi pocket; while, the δ_1 and δ_2 bands seem to be degenerate at the M point with the band bottoms at 180 meV, developing two electron pockets around the zone corner. In addition, there is another weak feature (ω) around the Γ point, whose band top is about 50 meV below E_F. Along M-X [cut #2 in Fig. 2(d)], three bands cross E_F as well, which are further confirmed by the peaks in the corresponding MDC fitting and EDCs [Fig. 2(e)]. Taking into account the bottom positions of these bands, we can infer that these two electronlike bands around M are the δ_1 and δ_2 bands, respectively. Based on the band calculations presented in Fig. 4 later, the band near X (marked by blue dashed lines) is β.

Along Γ-X, data in Figs. 2(f) and 2(g) show a shallow electronlike band (blue dashed line). Based on the analysis presented in Fig. 4 later, this feature is actually contributed mostly by the β band. Such a shallow electronlike band is due to a pronounced hybridization between β and ω shown here. However, it does not develop into a closed electron pocket. Instead, it forms the narrow racetrack holelike Fermi pocket (β) surrounding X.

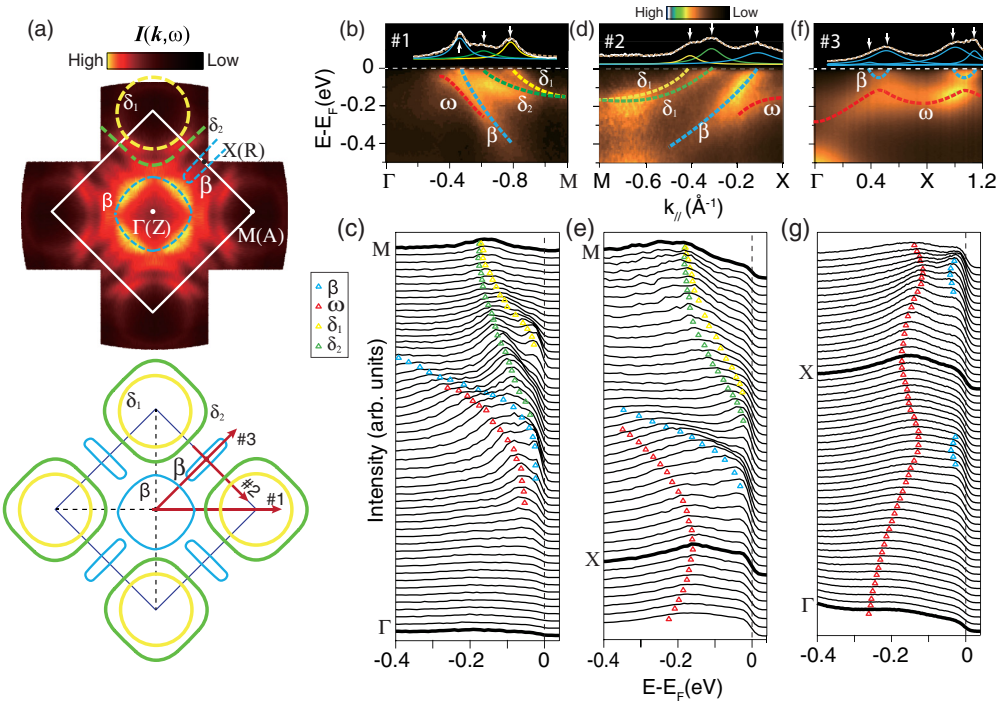

FIG. 2. (Color online) Electronic structure of KNi_2Se_2 measured at 15 K. (a) Photoemission intensity map integrated over ($E_F - 10$ meV, $E_F + 10$ meV) (upper panel) and the 2D projected Brillouin zone of KNi_2Se_2 (lower panel). It was obtained through mirroring the data with respect to both k_x and k_y axes. (b) The photoemission intensity along cut #1 (Γ-M direction). (c) Selected EDCs for data in (b). (d) and (e), (f) and (g) show similar data to that in (b) and (c), but along cut #2 and cut #3, respectively. The data in panel (a) were taken with randomly polarized 21.2 eV photons from a helium discharge lamp, and the other data were taken with circularly polarized 75 eV photons at KEK.

To fully reveal the Fermi surface topology in the three-dimensional Brillouin zone, we have performed detailed photon energy dependent ARPES measurements. Along cut #1, only the β band shows up in the s polarization [Fig. 3(a)]. The Fermi momenta (k_F's) of β are determined by peak positions in MDCs in Fig. 3(d). Taking the inner potential of 15 eV to estimate the k_z's for different photon energies, we notice that k_F's of β move periodically from Γ (probed with 21 eV photons) to Z (probed with 31 eV photons). Our data could cover more than half of the Brillouin zone along the k_z direction. On the other hand, δ_2 is clearly resolved in the p polarization [Fig. 3(b)], which shows negligible k_z dispersion [Fig. 3(e)]. Along cut #2, β and δ_1 band show up in the p polarization [Fig. 3(c)]. As shown in Fig. 3(f), there is some dispersion along k_z for the δ_1 band. In general, the k_z dispersions of these bands are not strong, manifesting the 2D nature of KNi_2Se_2. Our result is consistent with the previous theoretical calculations except for the holelike pocket centered at the Γ point, which was suggested to be more three-dimensional-like [19,20]. This discrepancy might be partially attributed to the poor k_z resolution in ARPES experiments.

IV. DISCUSSIONS AND CONCLUSIONS

The measured quasi-2D electronic structure of KNi_2Se_2 is compared with the band structure obtained from our first-principles calculations. In Fig. 4, the calculated bands (dashed lines) are scaled and appended onto the photoemission intensity plots along the three high-symmetry directions. Here, a renormalization factor of about 1.54 to the calculations leads to a remarkable agreement with the experimental data. Almost all characteristic dispersions, even the small electronlike feature along the Γ-X direction, can be reproduced well by the calculations. The relatively small renormalization factor demonstrates that the electron correlations in this system are weak. In addition, our calculation results show that the adjacent bands (δ_1, δ_2, ω, and β) near E_F strongly hybridize with each other along the Γ-M direction. We present the calculated total DOS and the projected DOS of KNi_2Se_2 in the right panel of Fig. 4, which indicates that the Se $4p$ orbitals also contribute DOS near E_F in addition to the dominating Ni $3d$ orbitals. Thus we could expect that the hybridizations of $3d$ Ni orbitals in KNi_2Se_2 are mediated by the relatively itinerant Se $4p$ orbitals.

The small renormalization factor found here for KNi_2Se_2 is similar to that of $BaNi_2As_2$ ($\sim$1.66) [12], which suggests that electron correlations are weak in both systems. This is consistent with their Ni orbital configurations, i.e., $3d^8$ for $BaNi_2As_2$, and $3d^{8.5}$ for KNi_2Se_2. Hund's rule coupling is the main source of correlations in these materials, and it has been shown recently that the correlations are reduced dramatically from $3d^6$ to $3d^7$ with electron doping, and superconductivity diminishes with weakened correlations [13]. Therefore, compared with the iron-based superconductors, the even higher $3d$ occupation and weaker correlations in these Ni-based compounds suggest that the superconductivity is most likely due to the electron-phonon coupling, similar to that in the multiband superconductor MgB_2 [21,22].

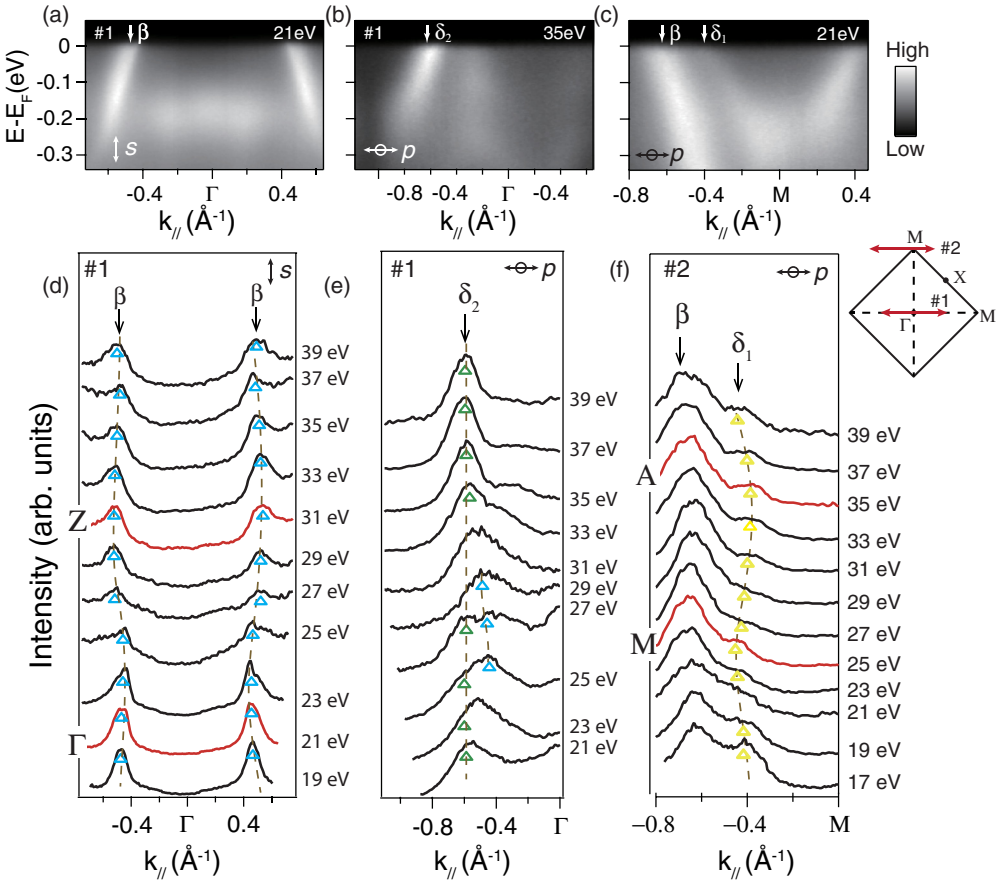

FIG. 3. (Color online) (a) The photoemission intensity taken along cut #1 with s polarized 21 eV photons. (b) The photoemission intensity taken along cut #1 with p polarized 35 eV photons. (c) is the same as (a) but along cut #2. (d) and (e) are MDCs at E_F taken with different photon energies along cut #1 in s and p polarizations, respectively. (f) is the same as (d) but taken along cut #2 in p polarization. The inset on the right shows the Brillouin zone of KNi_2Se_2 and the two solid lines mark cut #1 and cut #2. The data were taken at Beamline 7U of UVSOR, and the temperature was 66 K.

One of the most intriguing aspects of KNi_2Se_2 is the possible heavy electronic state existing below ~20 K (T_H), as mentioned in Ref. [10], with an enhanced effective electronic band mass. As no anomalous peak was observed at 20 K in other transport measurements, we think the change of γ here is not a very sharp phase transition, but a continuous transition. ARPES is a powerful technique to study phase transitions in which electronic structures change significantly, like SDW in iron-based superconductors [23,24], but unfortunately it has no sufficient precision/sensibility to detect the continuous transition of γ here. To avoid thermal broadening and assure the system is lying in the possible heavy electronic state, Fermi surface mappings and high-symmetrical photoemission intensities were all taken at 15 K in our experiments. However, the well-defined bands observed at 15 K and the weakly correlated electronic structure seems inconsistent with the proposed heavy electronic state.

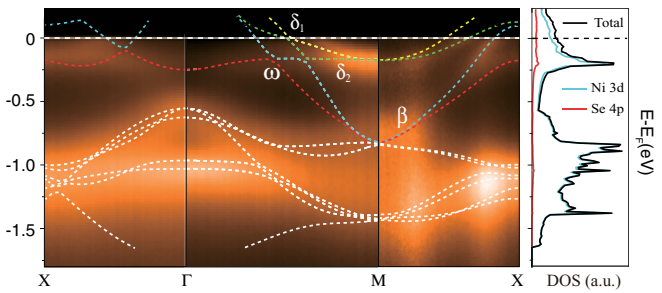

FIG. 4. (Color online) Left: Comparison of the ARPES experimental band structure and the DFT calculation results along the high-symmetry directions in KNi_2Se_2. Right: Calculated DOS of KNi_2Se_2, in which blue and red curves correspond to Ni and Se partial DOS, respectively.

To understand the origin of the large Sommerfield coefficient in KNi_2Se_2, we compare its specific heat and electronic structure with those of $BaNi_2As_2$ and KFe_2As_2. The latter has a Fe $3d^{5.5}$ orbital configuration, which fosters stronger Hund's rule coupling and higher electron correlations (renormalization factor 2–4) [25], leading to higher γ (94.3 mJ mol^{-1} K^{-2}) [16]. Meanwhile, the γ is 49.8 mJ mol^{-1} K^{-2} for KNi_2Se_2, and 13.2 mJ mol^{-1} K^{-2} for $BaNi_2As_2$ [15]. As the electronic specific heat γ coefficient is proportional to the DOS at E_F, which can be further estimated by the formula $\gamma \propto \sum_n \int_{s_n(E_F)} \frac{ds}{|\nabla_k E(k_F)|}$, where n is the band index, $|\nabla_k E(k_F)|$ is the mean velocity of an electron at E_F. For a 2D system, the formula can be simplified through $ds \rightarrow$ the perimeter of Fermi surface, and $|\nabla_k E(k_F)| \rightarrow$ the Fermi velocity or the

(a)

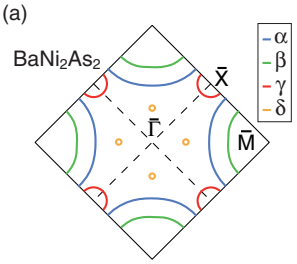

(b)

Band	Perimeter (P) Å^{-1}	Average Slope (V) eV•Å	P/V eV^{-1}• Å^{-2}	∑P/V eV^{-1}• Å^{-2}	γ coefficient mJ• K^{-2}•mol^{-1}
α	4.4(4)	2.0(2)	2.2(3)	4.2(4)	13.2
β	3.0(3)	2.3(2)	1.3(2)		
γ	1.5(1)	2.1(2)	0.7(1)		
δ	0.62(6)	8.2(8)	0.07(1)		

(c)

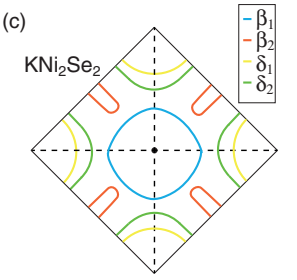

(d)

Band	Perimeter (P) Å^{-1}	Average Slope (V) eV•Å	P/V eV^{-1}• Å^{-2}	∑P/V eV^{-1}• Å^{-2}	γ coefficient mJ• K^{-2}•mol^{-1}
β_1	2.5(2)	1.4(1)	1.7(2)	17(2)	49.8
β_2	2.7(2)	1.2(1)	2.2(3)		
δ_1	2.5(2)	1.0(1)	2.5(4)		
δ_2	3.4(3)	0.43(4)	11(2)		

(e)

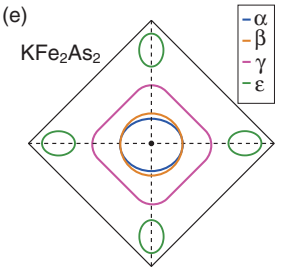

(f)

Band	Perimeter (P) Å^{-1}	Average Slope (V) eV•Å	P/V eV^{-1}• Å^{-2}	∑P/V eV^{-1}• Å^{-2}	γ coefficient mJ• K^{-2}•mol^{-1}
α	1.7(1)	0.56(5)	3.0(4)	31(3)	94.3
β	1.8(1)	0.96(9)	1.9(3)		
γ	3.3(3)	0.22(2)	15(2)		
ε	3.4(3)	0.29(2)	12(2)		

FIG. 5. (Color online) (a) Sketch of Fermi surface for $BaNi_2As_2$, reproduced from Ref. [12]. (b) The DOS estimation of each band in $BaNi_2As_2$ system. (c) and (d), (e) and (f) are the same as in panels (a) and (b), but for KNi_2Se_2 and KFe_2As_2, respectively. For distinguishing two β Fermi pockets in KNi_2Se_2, we sign the Fermi pocket around Γ as β_1 and around X as β_2 in panel (b).

band slope at E_F. Thus we can roughly evaluate the DOS at E_F of these systems, as shown in Fig. 5.

By estimation, we notice that the total Fermi surface perimeters are similar for all three systems [Figs. 5(a), 5(c), and 5(e)]. However, the average Fermi velocity decreases rapidly in the order of $BaNi_2As_2$, KNi_2Se_2, and KFe_2As_2 [Figs. 5(b), 5(d), and 5(f)]. Consequently, the estimated DOS value in KNi_2Se_2 is 4.0(6) times that of $BaNi_2As_2$, which is generally consistent with the corresponding ratio (3.8) of their γ coefficients. Similarly, both the estimated DOS and γ of KFe_2As_2 are about 1.8–1.9 times those of KNi_2Se_2. Therefore, our data suggest that the large γ in KNi_2Se_2 is due to the relatively flat bands (especially δ_2) in combination with the large Fermi surface perimeters. These are confirmed by our DFT calculations, which give flat δ_1 and δ_2. Although ω in KNi_2Se_2 is also relatively flat, it lies about 50 meV below E_F and contributes very little to the specific heat.

Our results also suggest that the large γ in KFe_2As_2 is not due to heavy-fermion physics, but due to strong correlations or Hund's rule coupling there as well. Furthermore, the good agreement between the estimated DOS at E_F and the measured γ for all three systems with different levels of correlation strength shows that this rough estimation of γ coefficients using photoemission data may possibly give a qualitative picture to understand the thermal dynamical properties of these multiband materials.

The neutron pair-distribution-function analysis revealed that the local CDW fluctuation occurs at T_H and disappears upon further cooling [1]. Temperature evolution of the electronic structure is shown in Fig. 6. The photoemission intensity along Γ-M (cut #1) is displayed in Fig. 6(b); we found that there is no evident spectral weight change with temperature within our energy resolution, except for some thermal broadening effects [Fig. 6(d)]. Along M-X (cut #2), as shown in Fig. 6(c), there is a spectral weight suppression with increasing temperature for δ_1, δ_2, and ω, as indicated by the up arrows in Fig. 6(e). Note that on the EDC's for momenta ④in Fig. 6(e), though the strong spectral weight around X originated from the band top of ω below E_F and β is hardly visible, likely due to matrix element effects, its suppression is rather evident. From the EDC's for momenta ⑤ and ⑥, we observed the sharp peaks of δ_1 and δ_2 appear at 11 K, which could be explained by the suppression of the thermal broadening effect. Moreover, the intensities of quasiparticle peaks from δ_1 and δ_2 at E_F decrease gradually upon warming. However, the spectral weight suppression rate does not alter noticeably across T_H. Similar spectral weight change was observed in $Sr_2CuO_2Cl_2$ and $BaTi_2As_2O$, which is explained by strong coupling between electrons and magnons or phonons [26,27]. For $BaTi_2As_2O$, a change of the spectral weight evolution rate was observed at the CDW ordering temperature. The absence of anomaly at T_H here is likely due to the fact that the CDW fluctuation in KNi_2Se_2 was

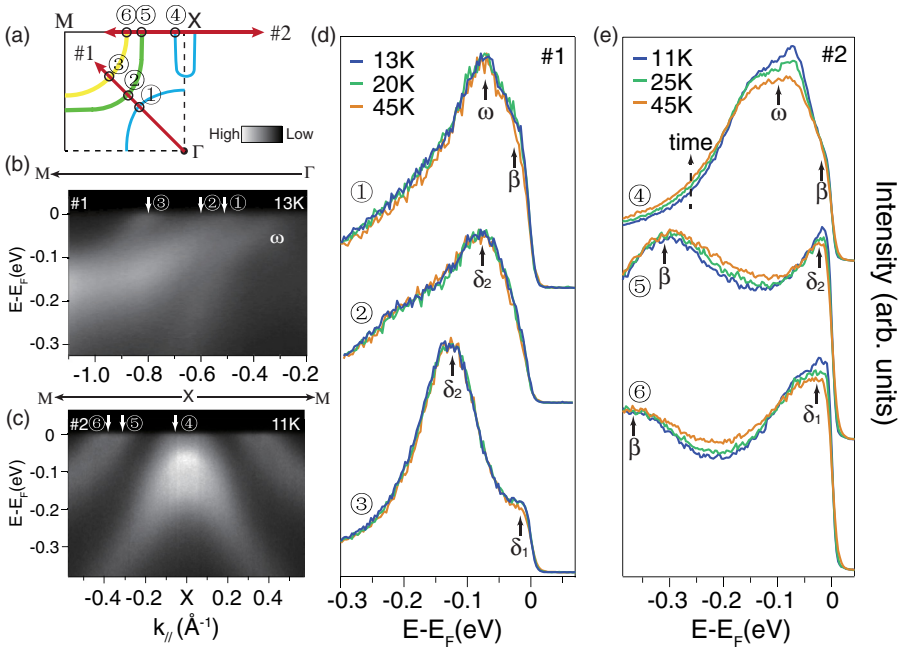

FIG. 6. (Color online) (a) The sketch of a Brillouin zone quadrant. (b) and (c) Photoemission intensities along cuts #1 and #2 as indicated in panel (a), respectively. (d) and (e) Temperature dependence of EDC¡¯s at various momenta as marked in panel (a). The dashed arrow "time" means the temperature dependent experiment measured upon warming. The data in panels (b) and (d) were taken with circularly polarized 75 eV photons at KEK, and the other data were taken with randomly polarized 21.2 eV photons from a helium discharge lamp.

reported to be dynamic and/or entirely uncorrelated between unit cells within the *ab* plane, in contrast to the coherent CDWs observed in structurally related compounds such as $NbSe_2$ [28]. Nevertheless, since we observed spectral weight suppression at nested Fermi surface sections, it may indicate that the enhanced electron-phonon interactions in these sectors may be responsible for the local CDW fluctuations.

To summarize, we have systematically studied the electronic structure of KNi_2Se_2 by high-resolution ARPES. There are three bands intersecting the Fermi level, which form two electronlike pockets, one squarelike, and one elongated elliptical holelike pocket surrounding the M, Γ, and X points, respectively. Furthermore, the electronic structure of this multiorbital superconductor shows relatively weak k_z dependence, indicative of its 2D nature. Further comparison with the DFT band calculations suggests that the electron correlations therein are relatively weak. Our results clearly indicate that it is not the heavy-fermion behavior advocated before, but the relative small Fermi velocities of bands in combination with large Fermi surfaces that lead to the large DOS and electronic specific heat coefficient in KNi_2Se_2. We also practiced aother way to quantitatively estimate DOS from ARPES data, which would provide valuable insight for understanding the thermal dynamic properties. Moreover, we observed intriguing temperature dependence of the electronic structure in the nested Fermi surface sectors, although we did not observe evident anomaly across T_H. This may be consistent with the local fluctuating CDW in KNi_2Se_2.

ACKNOWLEDGMENTS

We gratefully acknowledge the helpful discussions with Professor Xiangang Wan. This work was supported by National Basic Research Program of China (973 Program) under Grants No. 2011CBA00106, No. 2011CBA00112, and No. 2012CB927401, and the National Science Foundation of China under Grants No. 11104304, No. 11227902, and No. 11274332. M.Y.L. and D.W.S. are also supported by the "Strategic Priority Research Program (B)" of the Chinese Academy of Sciences (Grant No. XDB04040300).

[1] J. G. Guo, S. F. Jin, G. Wang, S. C. Wang, K. X. Zhu, T. T. Zhou, M. He, and X. L. Chen, Phys. Rev. B **82**, 180520(R) (2010).

[2] H. D. Wang, C. H. Dong, Z. J. Li, Q. H. Mao, S. S. Zhu, C. M. Feng, H. Q. Yuan, and M. H. Fang, Europhys. Lett. **93**, 47004 (2011).

[3] M. H. Fang, H. D. Wang, C. H. Dong, Z. J. Li, C. M. Feng, J. Chen, and H. Q. Yuan, Europhys. Lett. **94**, 27009 (2011).

[4] W. Bao, Q. Z. Huang, G. F. Chen, M. A. Green, D. M. Wang, J. B. He, and Y. M. Qiu, Chin. Phys. Lett. **28**, 086104 (2011).

[5] F. Ye, S. Chi, W. Bao, X. F. Wang, J. J. Ying, X. H. Chen, H. D. Wang, C. H. Dong, and M. H. Fang, Phys. Rev. Lett. **107**, 137003 (2011).

[6] Y. J. Yan, M. Zhang, A. F. Wang, J. J. Ying, Z. Y. Li, W. Qin, X. G. Luo, J. Q. Li, J. P. Hu, and X. H. Chen, Sci. Rep. **2**, 212 (2012).

[7] H. H. Wen, Rep. Prog. Phys. **75**, 112501 (2012).

[8] T. Qian, X. P. Wang, W. C. Jin, P. Zhang, P. Richard, G. Xu, X. Dai, Z. Fang, J. G. Guo, X. L. Chen, and H. Ding, Phys. Rev. Lett. **106**, 187001 (2011).

[9] Y. Zhang, L. X. Yang, M. Xu, Z. R. Ye, F. Chen, C. He, H. C. Xu, J. Jiang, B. P. Xie, J. J. Ying, X. F. Wang, X. H. Chen, J. P. Hu, M. Matsunami, S. Kimura, and D. L. Feng, Nat. Mater. **10**, 273 (2011).

[10] J. R. Neilson, A. Llobet, A. V. Stier, L. Wu, J. J. Wen, J. Tao, Y. M. Zhu, Z. B. Tesanovic, N. P. Armitage, and T. M. McQueen, Phys. Rev. B **86**, 054512 (2012).

[11] H. C. Lei, M. Abeykoon, K. F. Wang, E. S. Bozin, H. Ryu, D. Graf, J. B. Warren, and C. Petrovic, J. Phys.: Condens. Matter **26**, 015701 (2014).
[12] B. Zhou, M. Xu, Y. Zhang, G. Xu, C. He, L. X. Yang, F. Chen, B. P. Xie, X. Y. Cui, M. Arita, K. Shimada, H. Namatame, M. Taniguchi, X. Dai, and D. L. Feng, Phys. Rev. B **83**, 035110 (2011).
[13] Z. R. Ye, Y. Zhang, F. Chen, M. Xu, J. Jiang, X. H. Niu, C. H. P. Wen, L. Y. Xing, X. C. Wang, C. Q. Jin, B. P. Xie, and D. L. Feng, Phys. Rev. X **4**, 031041 (2014).
[14] J. R. Neilson and T. M. McQueen, J. Am. Chem. Soc. **134**, 7750 (2012).
[15] A. S. Sefat, M. A. McGuire, R. Jin, B. C. Sales, D. Mandrus, F. Ronning, E. D. Bauer, and Y. Mozharivskyj, Phys. Rev. B **79**, 094508 (2009).
[16] M. Abdel-Hafiez, S. Aswartham, S. Wurmehl, V. Grinenko, C. Hess, S. L. Drechsler, S. Johnston, A. U. B. Wolter, B. Büchner, H. Rosner, and L. Boeri, Phys. Rev. B **85**, 134533 (2012).
[17] G. Kresse and J. Furthmuller, Phys. Rev. B **54**, 11169 (1996).
[18] J. P. Perdew, K. Burke, and M. Ernzerhof, Phys. Rev. Lett. **77**, 3865 (1996).
[19] F. Lu, J. Z. Zhao, and W. H. Wang, J. Phys.: Condens. Matter **24**, 495501 (2012).
[20] V. V. Bannikov and A. L. Ivanovskii, Physica B **418**, 76 (2013).
[21] I. I. Mazin, O. K. Andersen, O. Jepsen, O. V. Dolgov, J. Kortus, A. A. Golubov, A. B. Kuz'menko, and D. van der Marel, Phys. Rev. Lett. **89**, 107002 (2002).
[22] H. Uchiyama, K. M. Shen, S. Lee, A. Damascelli, D. H. Lu, D. L. Feng, Z. X. Shen, and S. Tajima, Phys. Rev. Lett. **88**, 157002 (2002).
[23] C. He, Y. Zhang, B. P. Xie, X. F. Wang, L. X. Yang, B. Zhou, F. Chen, M. Arita, K. Shimada, H. Namatame, M. Taniguchi, X. H. Chen, J. P. Hu, and D. L. Feng, Phys. Rev. Lett. **105**, 117002 (2010).
[24] Y. Zhang, C. He, Z. R. Ye, J. Jiang, F. Chen, M. Xu, Q. Q. Ge, B. P. Xie, J. Wei, M. Aeschlimann, X. Y. Cui, M. Shi, J. P. Hu, and D. L. Feng, Phys. Rev. B **85**, 085121 (2012).
[25] T. Sato, K. Nakayama, Y. Sekiba, P. Richard, Y. M. Xu, S. Souma, T. Takahashi, G. F. Chen, J. L. Luo, N. L. Wang, and H. Ding, Phys. Rev. Lett. **103**, 047002 (2009).
[26] C. Kim, F. Ronning, A. Damascelli, D. L. Feng, Z. X. Shen, B. O. Wells, Y. J. Kim, R. J. Birgeneau, M. A. Kastner, L. L. Miller, H. Eisaki, and S. Uchida, Phys. Rev. B **65**, 174516 (2002).
[27] H. C. Xu, M. Xu, R. Peng, Y. Zhang, Q. Q. Ge, F. Qin, M. Xia, J. J. Ying, X. H. Chen, X. L. Yu, L. J. Zou, M. Arita, K. Shimada, M. Taniguchi, D. H. Lu, B. P. Xie, and D. L. Feng, Phys. Rev. B **89**, 155108 (2014).
[28] D. W. Shen, B. P. Xie, J. F. Zhao, L. X. Yang, L. Fang, J. Shi, R. H. He, D. H. Lu, H. H. Wen, and D. L. Feng, Phys. Rev. Lett. **99**, 216404 (2007).